Proceedings of the
Annual Stability Conference
Structural Stability Research Council
Grapevine, Texas, April 18-21, 2012

Stability of sheathed cold-formed steel studs under axial load and bending

K.D. Peterman[1], B.W. Schafer[2]

Abstract
This research aims to identify and characterize the behavior of dissimilarly sheathed cold-formed steel (CFS) lipped channels (studs) under axial load and bending. These experiments are part of a larger effort to improve design methods and general understanding of CFS columns and their components, utilizing standard construction methods and sheathing configurations: Oriented Strand Board (OSB) and gypsum board. Previous work on sheathed studs and full-scale walls (Vieira, 2011) under axial compression alone demonstrated that sheathing on both sides of the member triggered a local buckling limit state and further restricted global and distortional modes. This was found to be true even for dissimilarly sheathed members, excepting walls and studs sheathed only on one side. In the tests conducted herein single CFS studs, sheathed with OSB or gypsum, or left bare (and any combination thereof on the two sides of the stud) are tested in axial compression and bending. Axial compression was applied to a pre-determined percentage of axial peak capacity (varying from 10% to 80% of the axial capacity of the stud) and then a horizontal load located at specimen mid-height was applied until failure. This configuration results in axial load, bending, and a direct torsion on the CFS stud. To stabilize the stud, tracks at the stud ends were clamped to the top and bottom of the testing rig to avoid liftoff during application of the horizontal load and to better simulate the response of full-walls, with multiple studs and wider sheathing. The immediate goal of the tests is to define the strength of similar and dissimilarly sheathed studs under combined loads. Sheathing type as well as configuration with respect to the loaded face was found to significantly effect the specimen response. Results are compared to nominal section strength. The combination experimental and analytical results will be utilized in full-scale CFS building experiments, modeling, and recommended changes to the AISI specification.

1. Test Setup

1.1 Testing Rig

The Johns Hopkins University multi-degree of freedom (MDOF) testing rig was used for this series of tests. The MDOF rig can load full-scale walls and columns with axial load, shear, and bending, although only axial load and bending were employed in this test series. Figure 1c depicts the MDOF rig with a single column specimen.

[1] Graduate Research Assistant, Department of Civil Engineering, Johns Hopkins University, <kpeterm1@jhu.edu>
[2] Professor and Chair, Department of Civil Engineering, Johns Hopkins University, <schafer@jhu.edu>

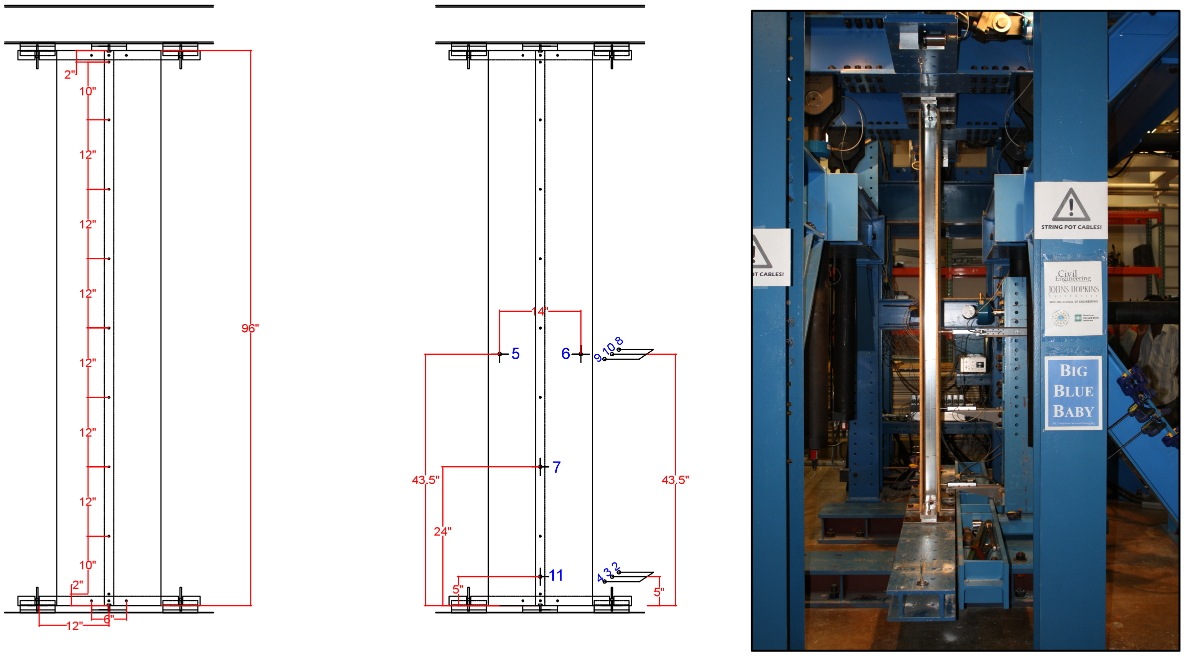

(a) (b) (c)

Figure 1: (a) Specimen design (b) Sensor plan (c) Side view of Johns Hopkins University MDOF testing rig

The specimen is connected to the loading beam on top and the 'ground' beam on bottom. Four hydraulic actuators apply axial load while one actuator applies bending moment in the form of a horizontal load at specimen mid-height.

1.2 Specimen Design and End Conditions

Sheathed single studs (362S162-068 [50ksi], SSMA nomenclature) connected to track (362T125-068) at the stud ends were constructed to approximate field studs in a typical 8ft-by-8ft cold-formed steel shear wall. Figure 1(a) and (b) depicts the specimen design and fastener layout. Note that the distance from stud to sheathing edge is half of a typical 24 inch stud spacing, thus encompassing the sheathing acted upon by a single stud. The two types of sheathing used in this test series were 7/16" oriented strand board (24/16 rated, exposure 1) and gypsum board (1/2" sheetrock). Simpson Quikdrive No. 6 x 1⅝" fasteners were used for attaching gypsum to the stud while Simpson Quikdrive No. 8 x 1 15/16" were used for the oriented strand board (OSB). The boards were stored in the JHU laboratory with an average humidity of 56% and temperature of 22°C (71°F) over 102 days.

Seven different sheathing combinations were tested: OSB-OSB (OO), gypsum-gypsum (GG), OSB-gypsum (OG), gypsum-OSB (GO), OSB-bare (OB), and bare-OSB (BO). In the nomenclature used, the right-hand letter signifies the loaded face of the specimen (for example, a GO specimen was loaded on the OSB side). It should be noted that in the specimens left bare on the loading face, the load was applied directly to the stud.

Special consideration of the column end conditions was required to best approximate a continuous full wall. In a full wall, the track connected to field studs is restricted from twist by virtue of being connected to adjacent studs. To simulate this behavior, track ends were clamped to the base and load beam of the MDOF testing rig via steel plates that blocked the track from movement. This clamping system used to fix the track ends to the machine is drawn in Figure 2.

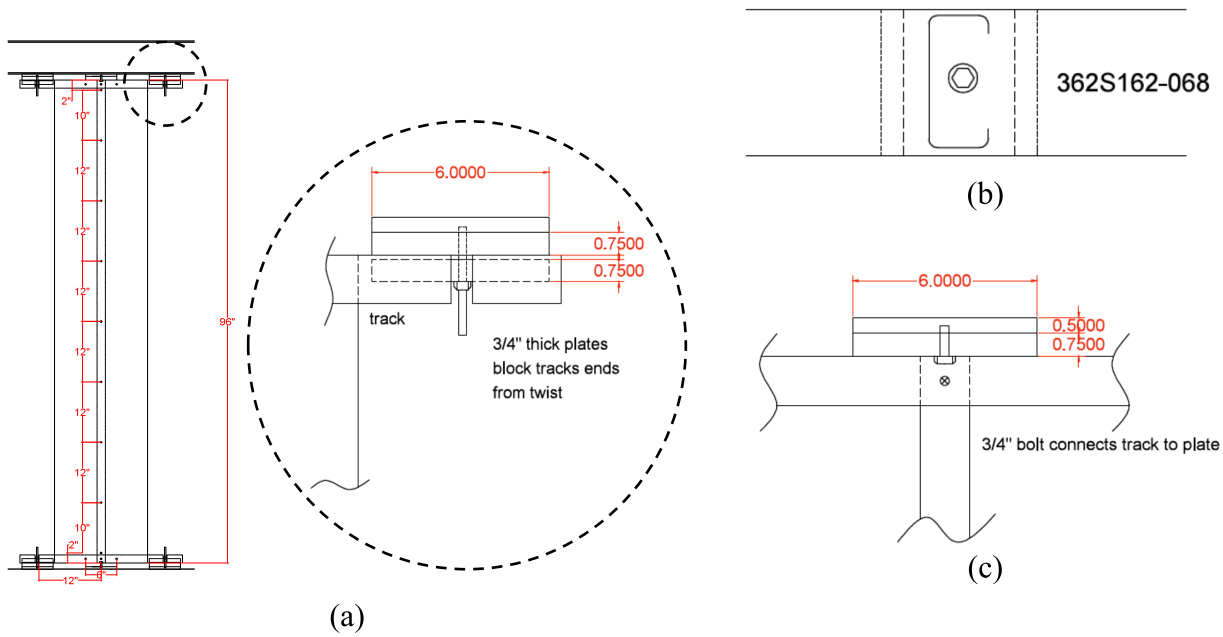

Figure 2: Drawings of end conditions, units of inches (a) track clamping system (b) plan view of stud-to-track connection (c) side view of stud-to-track connection

1.3 Sensor Plan

Thirteen sensors were employed to measure the response of the specimen under load. Eleven position transducers were connected to the specimen itself and two string potentiometers were connected to the testing rig alone to accurately capture machine displacement (refer to sensor plan in Figure 1b). Position transducers 5 and 6 capture twist in the sheathing and in combination with 7 and 11, record column displacement in the direction of the horizontal load application. To record motion of the stud during loading, sensors were arranged as triplets (9, 10, 8 and 4, 3, 2) and captured relative twist of the stud and local buckling waves in the middle of the stud web.

1.4 Load Protocol

Figure 3 demonstrates an idealization of the specimen under both axial load (P) and horizontal load (H). With this configuration, and assuming fixed end conditions, maximum moment exists at the center. The quantities in Figure 3 are relatively easy to discern, with the exception of torsion, due to the inherent difficulty in obtaining the eccentricity (e) of the load application point to the shear center of the cross-section. This will be discussed further in Section 1.5.

Two load protocols were employed in this series of testing. The first, used for a majority of the specimens, involved loading the stud with a pre-determined percentage of its axial capacity determined from previous stud tests (Shifferaw, et al. 2010) and then loading the stud at mid-height with a horizontal load until failure. The axial load was allowed to degrade as the horizontal load increased. The dashed line in Figure 4 represents this protocol.

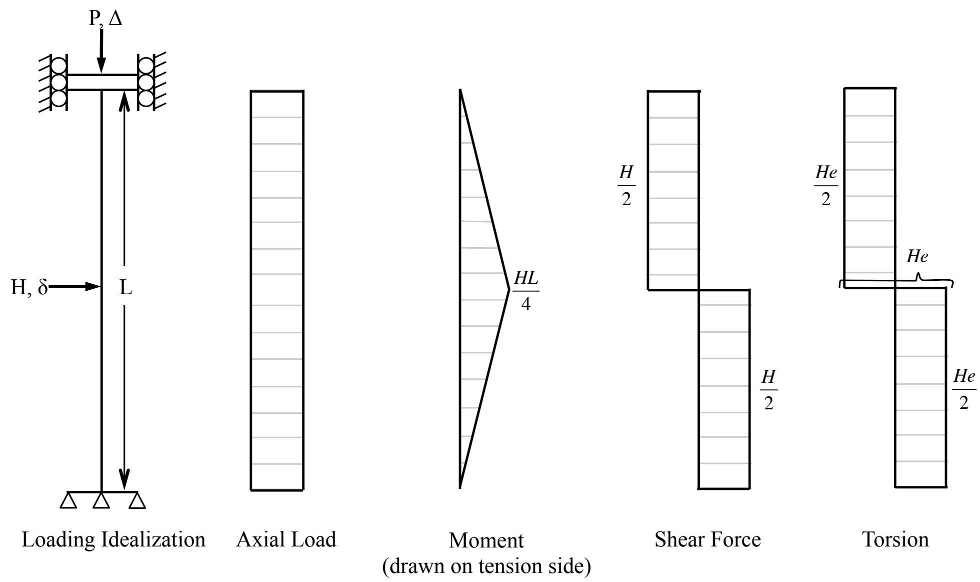

Figure 3: Loading and response idealization

In the second protocol, the constant axial displacement protocol, axial load is maintained as horizontal displacement increases. Once the stud has attained the pre-determined percentage of axial load, horizontal displacement and additional axial displacement are applied together such that axial load remains approximately constant. Only two specimens were loaded in this manner to achieve a true 80% of P_{max} at failure, rather than the lower percentage. Figure 4 compares the two protocols for specimens loaded via the first protocol (constant axial displacement, specimen S39-GG) and the second (constant axial load, specimen S30-GG).

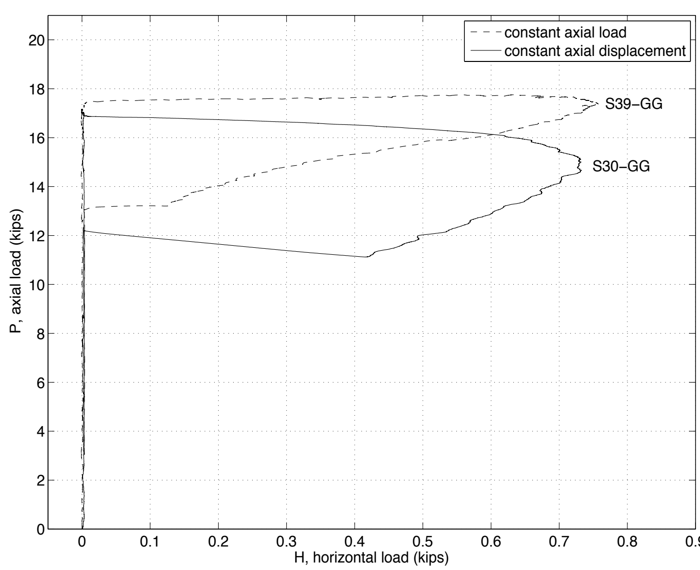

Figure 4: Plot of P-M space for two GG specimens with differing load protocols

In the case of the constant axial displacement protocol, axial displacement was applied at an average rate of 0.2 in. over 5 minutes, or 0.04 in./min. It should be noted that this loading rate was not enforced with particular diligence, and varies slightly from specimen to specimen, based on machine location and desired axial load. However, in specimens taken to larger axial load values, loading rate was decreased so as to not fail the specimens (via rapid load rate) before their pre-determined peak axial capacity. The rate at which horizontal load was applied was enforced at 1.5” over 32 minutes, or 0.0469in./min. The specimen was loaded until past peak.

1.5 Load Location

While the location of the horizontal load H along the length of the specimen has been discussed, the point at which the load is applied to the cross-section must not be neglected. This is represented in Figure 7 and discussed in Section 6.1 in detail. This location is not static and may dramatically change throughout the duration of a test. The test begins with the load bar pushing against the flat portion of the stud flange. Increasing horizontal load causes torsion in the specimen and the stud twists such that the load bar is directly in contact with the flange-web corner and in extreme cases (for unsheathed specimens), even the web flat. In sheathed specimens, this phenomenon is difficult to observe because the OSB or gypsum board obscures the stud face. In specimens without sheathing on the loading side (SXX-XB), contact between stud and load bar is etched onto the stud surface.

2. Test Matrix

A test matrix (Table 1) was constructed in an attempt to define the interaction space (axial load versus bending—the P-M space) for studs sheathed with combinations of OSB, gypsum, and no sheathing at all. The shaded area refers to a series of tests performed in Vieira et al. (2010) at Johns Hopkins University.

Table 1: Test Matrix

Loading		**Sheathing** (B=Bare, G=Gypsum, O=OSB)						
P	**H**	**BB**	**OB**		**GG**	**OG**		**OO**
100%	0	5 (2')	18 (2')		19 (2')	20 (2')		21 (2')
		6 (4')	14 (4')		15 (4')	16 (4')		17 (4')
		7 (6')	12 (6')		10 (6')	13 (6')		9 (6')
		22 (8')	23 (8')		25 (8')	24 (8')		26 (8')
P	**H**	**BB**	**OB**	**BO**	**GG**	**OG**	**GO**	**OO**
~80%P	to failure	xx	xx	xx	S39	xx	xx	S18
$\Delta_{80\%P}$	to failure	xx	S21	S37	S23,S30	S32	S16	S15
$\Delta_{60\%P}$	to failure	S34	S14	S27	S20	S36	S08	S38
$\Delta_{40\%P}$	to failure	S26	S10	S13	S19	S05	S09	S01
$\Delta_{10\%P}$	to failure	xx	S06	xx	S12	S07	S33	S11

Legend:

(shaded)	Refers to existing test results of Vieira and Schafer, Vieira et al. first number is index, second number is length
xx	This configuration not tested
S#	This test series (Peterman and Schafer)

B=Bare, no sheathing

G=1/2 in. gypsum board fastened with #6 Simpson Strong Tie fasteners at 12 in. o.c.

O=7/16 in. OSB board fastened with #8 Simpson Strong Tie fasteners at 12 in. o.c.
OB = OSB on west side, Bare on East Side (load applied) --> BO = Bare on west side, OSB on East Side (load applied)

3. Material Properties and Cross-Section

Each stud tested was measured at three locations along their length (corresponding approximately to third-points) and dimensions were averaged across 40 measured specimens. Stud thickness, out-to-out dimensions, corner radii and corner angles were measured. Figure 5 depicts a representation of an idealized cross-section with SSMA dimensions and a cross-section with the average measurements taken from the test specimens, as well as measurements from an identical section in Vieira et al.

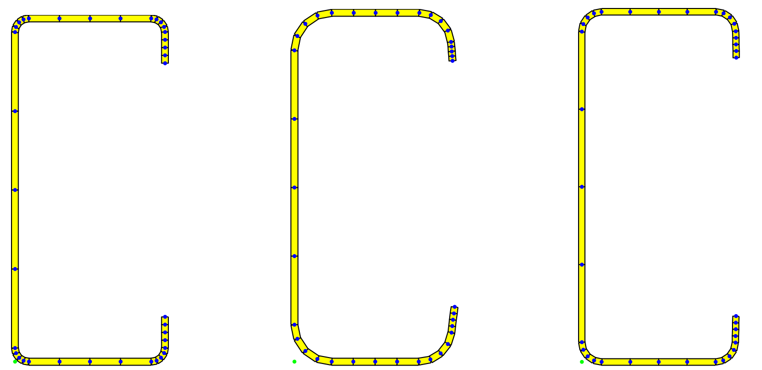

Figure 5 CUFSM models, drawn to scale, used for cross-section elastic buckling analysis (note, t=0.0715 in. and F_y= 59.9 ksi in the as-measured sections for this study, while t=0.0656 in. and F_y=55.5 ksi for the as-measured of Vieira et al., see Section 3 and 4 of this report for full details of the as-measured dimensions for this study)

4. Results

Test results are presented in Table 2 below. Boundary values are provided for perfectly pinned and fixed conditions.

Table 2: Result Summary

Nominal Loading		**Sheathing** (B=Bare, G=Gypsum, O=OSB)													
P	**H**	**BB**		**OB**				**GG**		**OG**				**OO**	
		L (ft)	**P_{test}** (kips)		**L** (ft)	**P_{test}** (kips)		**L** (ft)	**P_{test}** (kips)		**L** (ft)	**P_{test}** (kips)		**L** (ft)	**P_{test}** (kips)
100%	0	2'	19.8 (D)		2'	21.4 (L)		2'	21.7 (L)		2'	22.0 (L)		2'	22.8 (L)
		4'	19.0 (FT)		4'	22.0 (L)		4'	22.4 (L)		4'	21.6 (L)		4'	22.3 (L)
		6'	13.6 (FT)		6'	18.0 (FT)		6'	19.9 (L)		6'	20.5 (L)		6'	22.4 (L)
		8'	12.8 (F)		8'	15.6 (FT)		8'	21.4 (L)		8'	22.4 (L)		8'	23.1 (L)
		BB		**OB**		**BO**		**GG**		**OG**		**GO**		**OO**	
		P_{test} (kips)	**H_{test}** (kips)	**P_{test}** (kips)	**H_{test}** (kips)	**P_{test}** (kips)	**H_{test}** (kips)	**P_{test}** (kips)	**H_{test}** (kips)	**P_{test}** (kips)	**H_{test}** (kips)	**P_{test}** (kips)	**H_{test}** (kips)	**P_{test}** (kips)	**H_{test}** (kips)
~80%P	to failure	xx	xx	xx	xx	xx	xx	17.38	0.76	xx	xx	xx	xx	18.19	1.06 (L,FS)
$\Delta_{80\%P}$	to failure	xx	xx	9.92	0.96 (T)	11.41	0.73 (PT,T)	14.55	0.72 (PT,B)	15.29	1.00 (L,PT)	14.69	1.14 (PT,B)	14.93	1.34 (L,PT)
$\Delta_{60\%P}$	to failure	6.41	0.54 (T)	6.50	0.76 (PT)	7.20	0.78 (PT)	11.61	0.99 (PT,B)	10.14	1.17 (PT)	10.16	1.46 (B,L)	11.45	1.50 (L,PT)
$\Delta_{40\%P}$	to failure	2.39	0.59 (T)	4.57	0.76 (PT,T)	4.52	1.08 (PT,T)	6.84	1.09 (PT,B)	6.71	1.30 (L,PT)	7.46	1.54 (PT,B)	7.57	1.55 (L)
$\Delta_{10\%P}$	to failure	xx	xx	0.50	1.12 (T)	xx	xx	1.74	1.23 (PT,B)	1.73	1.38 (L,B,T)	1.82	1.63 (PT,L,B)	2.43	1.66 (L)

Legend

	L.C.M. Vieira Jr. et al. / Journal of Constructional Steel Research 67 (2011) 1554–1566
xx	This configuration not tested
##	This test series (Peterman and Schafer)

Sheathing

B=Bare, no sheathing

G=1/2 in. gypsum board fastened with #6 Simpson Strong Tie fasteners at 12 in. o.c.

O=7/16 in. OSB board fastened with #8 Simpson Strong Tie fasteners at 12 in. o.c.

OB = OSB on west side, Bare on East Side (load applied) --> BO = Bare on west side, OSB on East Side (load applied)

Failure Mode

L = Local buckling, D = Distortional buckling, FT = Flexural-torsionl buckling

T = torsional failure, PT = fastener pull-through, B = fastener bearing

5. Analysis

This section provides member and fastener capacities that later may be used to compare to the testing. The direct comparison to the testing requires some consideration of the end conditions and the manner in which the fasteners are loaded – these issues are taken up in Section 8 where the comparisons are provided, this section just provides basic capacity.

5.1 Local Buckling Member Capacity

The upper bound capacity of the sheathed stud is the local buckling capacity. In the axial load tests of Vieira (2011) local buckling controlled the strength. If it is presumed that only local buckling controls (note this is not the case in the observed tests as fastener limit states and torsion were generally observed, but this is the upper bound strength), then: check only local buckling, i.e., no distortional buckling, no global buckling, no torsion, and no fastener failure. Under these assumptions C_m=1 and α=1, therefore a simplified version of the AISI-S100 interaction equations (C5.2) may be used. AISI-S100-07 provides an Effective Width approach in the main Specification (largely, Chapter B) and the Direct Strength approach in the Appendix (Appendix 1). Table 3 provides P_n and M_n for the nominal and as-measured dimensions and properties.

Table 3 Capacity of 362S162-68 (50 ksi) for local buckling

		Capacity in Compression and Bending[6]		
		dimensions and properties based on		
	Provision	**Nominal**	Peterman and Schafer Beam-column tests **As-measured**	Vieira et al. Axial only tests **As-measured**
P_n	Main Spec.	20.2 kips[1]	-[5]	-[5]
	DSM (App. 1)	23.7 kips[2]	28.0 kips[3]	22.2 kips[4]
M_n	Main Spec	28.7 in.-kips[1]	-[5]	-[5]
	DSM (App. 1)	29.5 in.-kips[2]	34.5 in.-kips[3]	30.6 in.-kips[4]

[1] AISI (2008) Table III-2 for P_n and AISI (2008) Table II-2 for M_n

[2] A_g=0.524 in^2, S_g=0.590 in^3 per SSMA (2010), P_{cr} = 31.7 kip, M_{cr} = 152.6 in.-kips per CFSEI G103-11 (2011), P_n and M_n found per AISI-S100-07 Appendix 1.

[3] t=0.0715in., A_g=0.522 in^2, S_g=0.577 in^3, F_y=59.9ksi, P_{cr} = 36.8 kip, M_{cr} = 196.9 in.-kips per CUFSM model of as-measured properties, P_n and M_n per AISI-S100-07 App. 1.

[4] t=0.0656in., A_g=0.484 in^2, S_g=0.5552 in^3, F_y=55.5ksi, P_{cr} = 24.7 kip, M_{cr} = 122.5 in.-kips per CUFSM model of as-measured properties, P_n and M_n per AISI-S100-07 App. 1.

[5] Not calculated.

[6] for nominal dimensions and properties note that P_{nd} and M_{nd} (per AISI 2008 Tables II-8 and III-5) are greater than P_n and M_n (for local buckling only) even with k_ϕ=0, so distortional buckling does not control.

5.2 Sheathing Braced Member Capacity

Member capacity is controlled by local, distortional, or global buckling (and/or combinations thereof). As discussed in detail in Vieira (2011) these buckling modes, particularly global buckling, may be influenced greatly by the presence of sheathing. Here we consider local buckling, distortional buckling, global buckling, but no direct torsion, and no fastener failure. Further we ignore the small second order amplification, therefore C_m=1 and α=1, and again a simplified version of the AISI-S100 interaction equations (C5.2) may be used. This is accomplished by determined the elastic critical local, distortional, and global buckling modes with appropriate springs modeling the fastener-sheathing stiffness. The approach can be modified for use in the main Specification of AISI-S100-07, but more easily follows from the Direct Strength approach in the Appendix (Appendix 1). Under the preceding assumptions P_n and M_n may be found according to DSM AISI S100.

The crucial step in the strength calculation via AISI-S100 Appendix 1 (Direct Strength) is the determination of the elastic buckling loads. This may be most easily accomplished with a finite strip analysis, using software such as CUFSM. CUFSM also provides a means to include the impact of springs. Based on the work of Vieira (2011) the stud-fastener-sheathing spring stiffness has previously been determined and is reported in Figure 6.

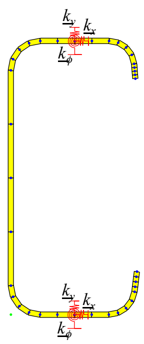

sheathing	spring	stiffness[1]		conversion to imperial		foundation stiffness for CUFSM[2]		
OSB	k_x	971	N/mm	5.52	kip/in.	$\underline{k}_x$	0.46	kip/in./in.
"	k_y	0.374	N/mm	0.0021	kip/in.	$\underline{k}_y$	0.00018	kip/in./in.
"	k_f	95309	Nmm/rad	0.84	kip-in./rad	$\underline{k}_f$	0.070	kip-in./rad/in.
Gyp	k_x	427	N/mm	2.43	kip/in.	$\underline{k}_x$	0.20	kip/in./in.
"	k_y	0.087	N/mm	0.00049	kip/in.	$\underline{k}_y$	0.000041	kip/in./in.
"	k_f	95987	Nmm/rad	0.85	kip-in./rad	$\underline{k}_f$	0.071	kip-in./rad/in.

(1) source: Vieira (2011) Table 6.3, fastener-stud-sheathing nominal dimensions and properties same as this testing

(2) as reported in Vieira (2011), fastener spacing of 12 in. used to convert to foundation stiffness for use in CUFSM

Figure 6 Fastener-sheathing stiffness (k's) for OSB and Gypsum, converted to foundation stiffness ($\underline{k}$'s)

The foundation stiffness values are included in a CUFSM 4.04 model of each of the cross-sections (Figure 5) and models are completed for both pinned and fixed end conditions with all sheathing configurations as reported in Table 4. In addition the elastic buckling values are used to determine the predicted capacity based on member buckling limit states via AISI-S100 Appendix 1 (Direct Strength Method) and also reported in Table 4.

Table 4 Nominal member capacity analysis including sheathing (using AISI-S100 Appendix 1 DSM)

			AXIAL						BENDING						
section	**end cond.**	**sheathing**	**sheathing**	**P_y** (kips)	**P_{crl}/P_y**	**P_{crd}/P_y**	**P_{cre}/P_y**	**P_n[1]** (kips)	**sheathing**	**M_y** (kip-in.)	**M_{crl}/M_y**	**M_{crd0}/M_y**	**M_{cre0}/M_y**	**C_bM_{cre0}/M_y**	**M_n[2]** (kip-in.)
as-measured	pinned	bare	BB	31.3	1.17	1.28	0.19	**5.2**	BB	35.5	5.70	2.35	0.37	0.48	**17.1**
Peterman &	"	one-sided	OB/BO	31.3	1.17	1.32	0.41	**11.2**	OB	35.5	>5.70	>2.35	0.80	1.06	**29.1**
Schafer	"	"							BO	35.5	>5.70	>2.35	>8	>8	**35.5**
"	"	two-sided	GG	31.3	1.17	1.35	1.01	**20.7**	GG	35.5	>5.70	>2.35	>8	>8	**35.5**
"	"	"	OG/GO	31.3	1.17	1.35	1.02	**20.7**	OG	35.5	>5.70	>2.35	>8	>8	**35.5**
"	"	"							GO	35.5	>5.70	>2.35	>8	>8	**35.5**
"	"	"	OO	31.3	1.17	1.36	1.04	**20.9**	OO	35.5	>5.70	>2.35	>8	>8	**35.5**
"	fixed	bare	BB	31.3	1.17	1.30	0.58	**15.2**	BB	35.5	>5.70	>2.35	1.23	1.63	**32.8**
"	"	one-sided	OB/BO	31.3	1.17	1.34	0.86	**19.2**	OB	35.5	>5.70	>2.35	1.52	2.00	**34.0**
"	"	"							BO	35.5	>5.70	>2.35	>8	>8	**35.5**
"	"	two-sided	GG	31.3	1.17	1.38	2.37	**24.8**	GG	35.5	>5.70	>2.35	>8	>8	**35.5**
"	"	"	OG/GO	31.3	1.17	1.38	2.56	**25.0**	OG	35.5	>5.70	>2.35	>8	>8	**35.5**
"	"	"							GO	35.5	>5.70	>2.35	>8	>8	**35.5**
"	"	"	OO	31.3	1.17	1.39	2.92	**25.4**	OO	35.5	>5.70	>2.35	>8	>8	**35.5**

(1) calculated per AISI-S100-07 Appendix 1 (DSM) with appropriate $\underline{k}x$, $\underline{k}y$, $\underline{k}f$ springs included in CUFSM4 models for finding Pcrl, Pcrd, Pcre

(2) calculated per AISI-S100-07 Appendix 1 (DSM) with appropriate $\underline{k}x$, $\underline{k}y$, $\underline{k}f$ springs included in CUFSM4 models for finding Mcrl, Mcrd, Mcre

(3) the number of longitudinal (*m*) terms kept in the CUFSM runs is as follows

nominal	1-10,33-39	for P runs	1-12,45-51	for M runs
as-measured	1-10,31-37	for P runs	1-11,39-45	for M runs
Vieira et al.	1-10,33-39	for P runs	1-11,44-50	for M runs

The results of Table 4 are extensive and the strength predictions will be evaluated further in Section 6; however, some items are worth noting.

- Overall the predicted strengths show similar progression in capacities as a function of sheathing as the testing.
- The presence of two-sided sheathing, whether it be gypsum board, OSB, or one of each greatly increases the predicted member capacities and even, to some extent, minimizes the importance of the end boundary conditions.

- Though not specifically noted on the table, for pinned end conditions in compression when two-sided sheathing is present the controlling global buckling mode is strong-axis buckling of the stud, thus one would consider the sheathing has successfully restricted weak-axis buckling and torsional(-flexural) buckling.
- For the 362S162-68 (50ksi) as a beam, local and distortional buckling should not control, instead global buckling is essentially the only relevant mode. (Note, the predictions do not include inelastic bending reserve, which may provide a modest boost to the predicted capacities in local and distortional buckling).

5.3 Fastener/Connection limit state capacities

Fastener nominal shear (P_{ss}) and tensile (P_{ts}) capacity are available from Simpson Strong Tie, yet exact fastener pull-through values are not directly available from industry reports. However, an alternative source of pull-through values exists in the rotational restraint tests of Vieira (2011). The tests were conducted on the same stud, fastener, and sheathing combinations as examined here. Maximum capacities were not reported in Vieira (2011) or the resulting paper (Schafer et al. 2009) so that data is provided in the test report corresponding to this paper (Peterman and Schafer 2012). Bearing values are available for the tested configurations (stud, fastener, and sheathing) in Vieira (2011). These fastener limit state capacities are compiled in Table 5.

Table 5 Summary of fastener-sheathing limit state capacities

	#8 in OSB	**#6 in Gypsum**
P_{ss}, Fastener shear[1]	1565 lbf	1260 lbf
P_{ts}, Fastener tension[1]	2160 lbf	1720 lbf
P_{pt}, Pull-through[2]	437 lbf	40 lbf
P_{br}, Bearing[3]	578 lbf	86 lbf

[1]Based on industry reported value, [2]Based on rotational restraint test, [3]Based on translational stiffness testing

6. Discussion

6.1 - Load Location

As briefly discussed in Section 1.6, the location of where the horizontal force H is applied to the specimen cross-section changes with the amount the stud twists. The bar begins loading at approximately the center of the flange. With a finite amount of twist, the bar remains on the flat width of the flange, but closer to the web-flange corner (Figure 7b). As this twist increases, however, the stud twists such that the bar applies load to the web-flange corner (Figure 7c).

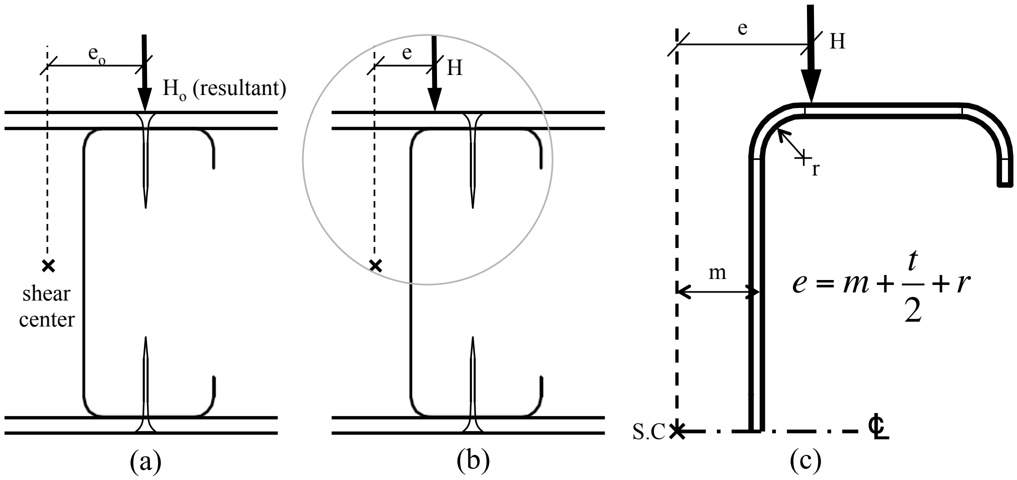

Figure 7: Load location cases (a) initial position (b) finite twist (c) detail of finite twist case

Determining torsional stresses on this cross-section can be convoluted in this instance, as the relationship of the load to stud shear center has dramatically changed. Despite this complexity, for any small, but finite twist, the authors suggest assuming a load location at the end of the flange flat width, nearest to the web-flange corner (Figure 7b) this is also consistent with studs directly loaded under small, but finite twist (see Figure 7b). So, $e = m + t/2 + r$, where e is the eccentricity of the load from the shear center, m is the distance from the shear center to the mid-plane of the web (as commonly tabled by SSMA, etc.) t is the design thickness, and r is the inner radius. For nominal dimensional properties of a 362S162-68:

$$e = m + t/2 + r = 0.765 \text{ in.} + 0.0713 \text{ in.}/2 + 0.1070 \text{ in.} = 0.91 \text{ in.}$$

6.2 - End Conditions

To accurately resolve the applied horizontal load into moments in the specimen, it is necessary to characterize the specimen end conditions. The intent of the detailed stud end conditions (see Section 1.3) was to simulate a stud in a complete wall system and the expectation, after previously conducted axial testing (Vieira 2011), was that this would supply fixed ends. Although the intent was met and the authors believe the stud-to-track-to-sheathing end condition is close to actual field conditions, the expectation of fixed end conditions was not met as the situation for members in bending is more complicated than members in compression.

To more definitively quantify the end boundary conditions the horizontal force (H) vs. the measured mid-height displacement (δ) was compared against theoretical fixed, pinned, and semi-rigid solutions in Figure 8. The theoretical fixed and pinned solutions are:

$$\text{fixed:} \quad \delta = \frac{HL^3}{192EI}, \quad k = \frac{192EI}{L^3} \tag{1}$$

$$\text{pinned:} \quad \delta = \frac{HL^3}{48EI}, \quad k = \frac{48EI}{L^3} \tag{2}$$

where nominal dimensions are employed for EI. The results (Figure 8) indicate that even under significant axial load the boundary conditions for bending about the major-axis of the stud are not fixed. In fact, for all cases pinned end boundary conditions are a more accurate estimate of the observed stiffness.

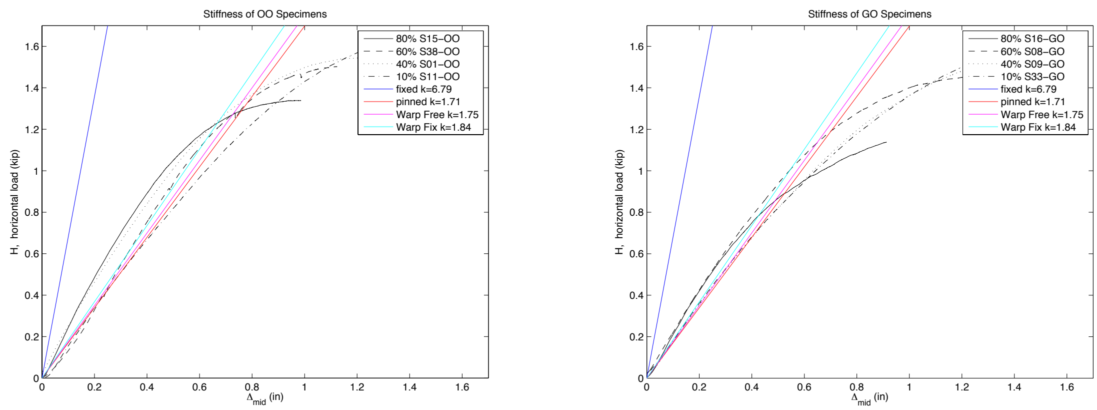

(a) (b)

Figure 8: Horizontal force vs. mid-height horizontal displacement with comparison to fixed, pinned, and semi-rigid end conditions from the short segment of connected track for (a) OO and (b) GO sheathed specimens

The results of Figure 8 also provide solutions for semi-rigid end conditions: warping free and warping fixed. These refer to boundary conditions on the short segment of track connected to the end of the studs. A beam element structural analysis model of the stud and track was created in MASTAN (Ziemian 2011) to assess the rotational stiffness supplied to the stud via twisting of the track. This model does not account for contact, but the stud is assumed to be perfectly connected to the track, while the track ends are modeled as either warping fixed or free. The moment for the pinned condition is HL/4 = 24 kip-in., the MASTAN results are nearly the same (23.7 and 22.9 kip-in. for warping free and fixed track ends respectively). Thus the authors conclude that the boundary conditions for major-axis bending is essentially pinned.

6.3 – Comparison of member limit states to tested capacity

The member limit state predictions of Table 4 are compared against the available test data in Figure 9. The impact of sheathing on the strength follows clear trends (Figure 9a) with the exception of the OB and BO tests, which undergo significant torsion. Although major-axis bending boundary conditions are shown to be essentially pinned in the previous section, the illustration of the necessity of assuming fixed end conditions under axial load is provided in Figure 9b. Weak-axis bending and torsion are sufficiently restricted to create fixed end conditions even for specimens without sheathing.

Although the test data of Table 2 and Figure 9a provides all the data together as they are nominally for the same 362S162-68 (50 ksi) stud the two test programs used different batches of studs. The results, as depicted in Figure 9c, show that while the specimens used for axial tests (Viera) are essentially identical to the nominal section, the specimens used in the testing reported herein (Peterman) are markedly stronger. Care must be taken when comparing predictions to the available data. The as-measured dimensions and properties of the Peterman specimens are used for subsequent analysis.

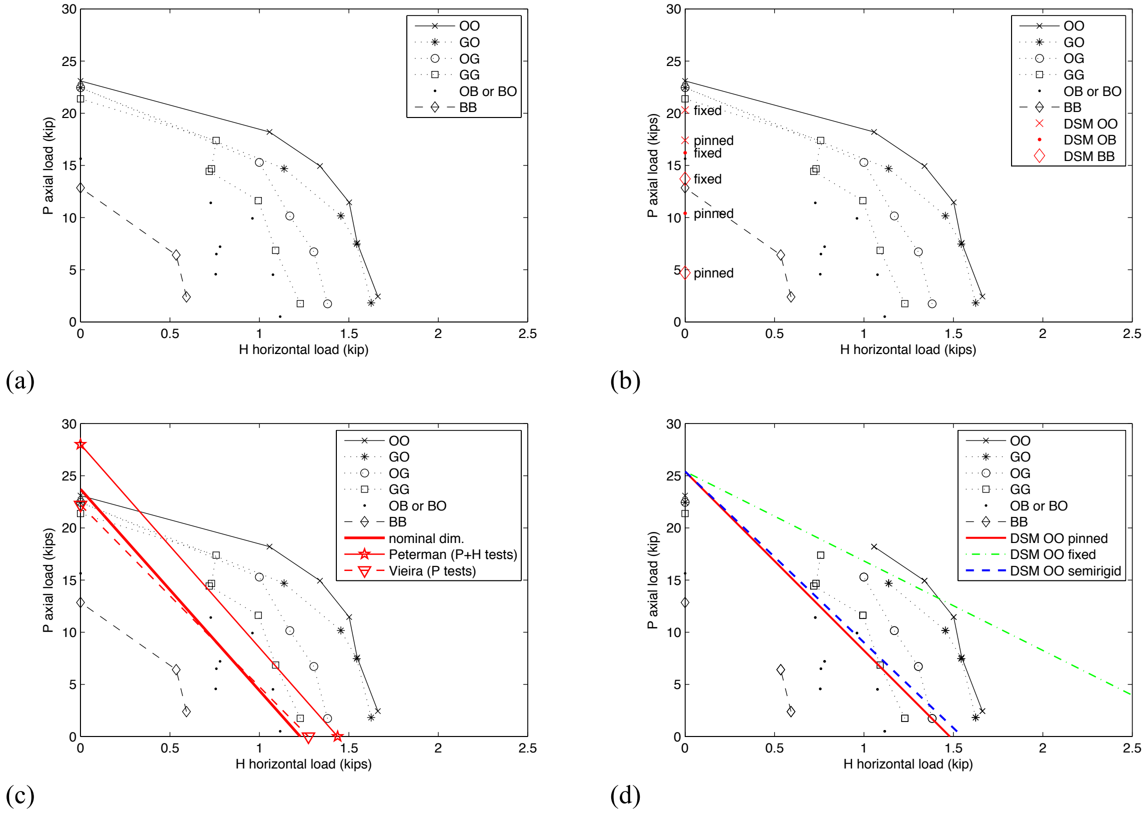

Figure 9 Axial load (P) and mid height horizontal load (H) at failure for 362S162-68 (50ksi) studs with various sheathing configurations (B=Bare, O=OSB, G=Gypsum), (a) raw data of Vieira (2011) and this study grouped by sheathing configuration, (b) comparison with predicted capacity for axial load tests of Vieira (2011) for different end conditions, (c) comparison with predicted local buckling capacity based on nominal dimensions and properties and as-measured dimensions and properties of Vieira (2011) and this study (Peterman), (d) comparison with predicted capacity of OO (OSB on both sides) Peterman specimens for various bending end boundary conditions.

Comparison of the impact of major-axis end boundary conditions is provided in Figure 9d for local buckling capacity of the Peterman as-measured sections. The importance of the end boundary conditions lies in whether or not the mid-height moment is HL/4 (pinned) or HL/8 (fixed). The previous section demonstrates that the end conditions are pinned. Thus, we see the important conclusion: all of the two-sided sheathing cases are able to develop their full member local buckling capacity with the exception of GG under high bending demands (which is modestly below the predicted member limit state).

Table 4 provides predicted member limit state capacities for all sheathing combinations. If we select the as-measured Peterman dimensions and properties, fixed end conditions for the axial capacities, and pinned end conditions for the bending capacities then the available data may be compared for all sheathing types as provided in Figure 10.

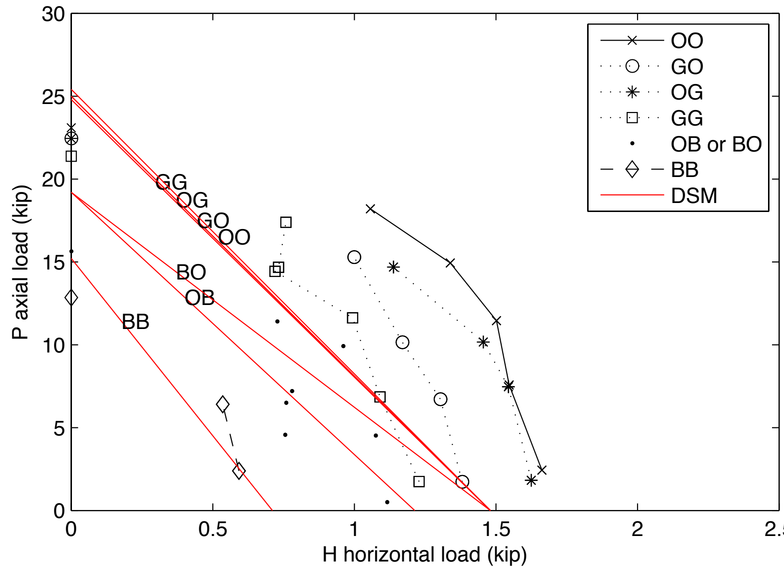

Figure 10 Axial load (P) and mid height horizontal load (H) at failure for 362S162-68 (50ksi) studs with various sheathing configurations (B=Bare, O=OSB, G=Gypsum) compared with predicted strength of Table 4 for Peterman sections, fixed end conditions for axial, pinned end conditions for bending

The Figure 10 results are encouraging. The bare specimens (BB) are conservatively predicted even though significant twist occurs. The specimens with one-sided sheathing (OB and BO) are reasonably predicted though significant scatter exists. All of the specimens sheathed on both sides are conservatively predicted with the exception of GG (gypsum on both sides) under high bending demands. Inelastic bending reserve and composite action (with respect to strength) are not included in the predicted strength and may account for the additional capacity observed in the additional specimens. In addition, fastener limit states are also addressed later in this paper.

6.4 – Role of fastener stiffness in determining fastener demand

It is typical in design to assume that the fastener-sheathing system will supply full torsional resistance to a sheathed member (stud), and thus the fasteners are designed to carry the full torsional moment. However, in reality the torsional stiffness of the fastener-sheathing system must be greater (significantly) than the member torsional stiffness, or the torsion will be borne by the member (as well as the twist!).

The member and fastener-sheathing attachments relevant for resisting torsion are provided in Figure 11. Here the springs are discrete (at each attachment location along the length of the member) with values as provided in Figure 6. To directly examine the impact of the fastener-sheathing stiffness the full system is turned into a single equivalent rotational spring,

$$k_\theta = k_{\phi 1} + \tfrac{1}{4} k_{x1} d^2 + k_{\phi 2} + \tfrac{1}{4} k_{x2} d^2 \tag{3}$$

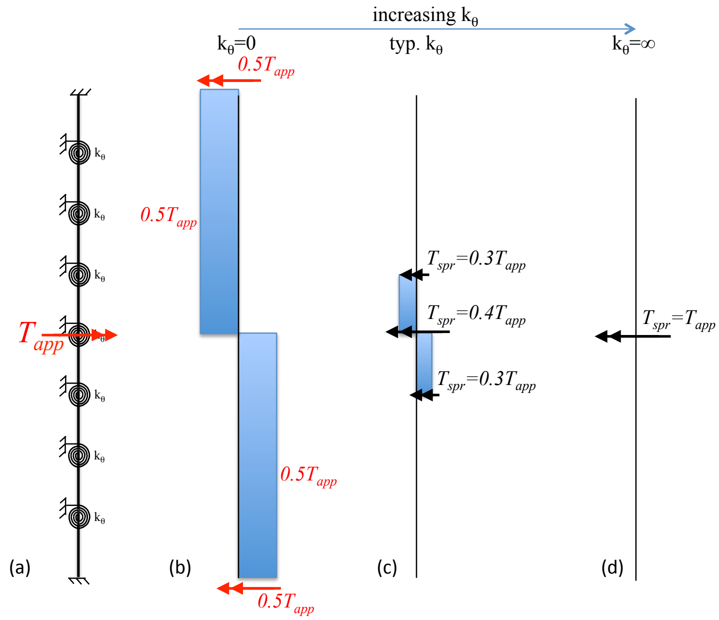

Figure 11 Torsional stiffness analysis model depicting (a) basic model, (b) torsional moment diagram without springs, (c) torsional moment diagram and spring forces for typical fastener-sheathing spring stiffness, (d) torsional moment diagram and spring force for infinitely stiff spring.

Noting that the member rotational stiffness ($k_{\theta\ member}$) is 3.2 kip-in./rad and that a bare stud of 96 in. in height with a 1 kip-in. unit torque at mid-height rotates (θ_{bare}) 0.312 rad (18 deg) a parametric study in MASTAN (Ziemian 2011) varying the 12 in. o.c. discretely spaced rotational spring k_θ from 0.01 kip-in./rad to 10,000 kip-in./rad is performed. The mid-height rotation and torsion in the spring at mid-height are reported in Figure 12. The behavior at the limits is consistent and understandable, but typical spring stiffness values lie in the middle. In this intermediate range the fasteners do not see the full torsional demand at the midspan fastener, but the result is the member twists – this is consistent with what was observed in the testing herein.

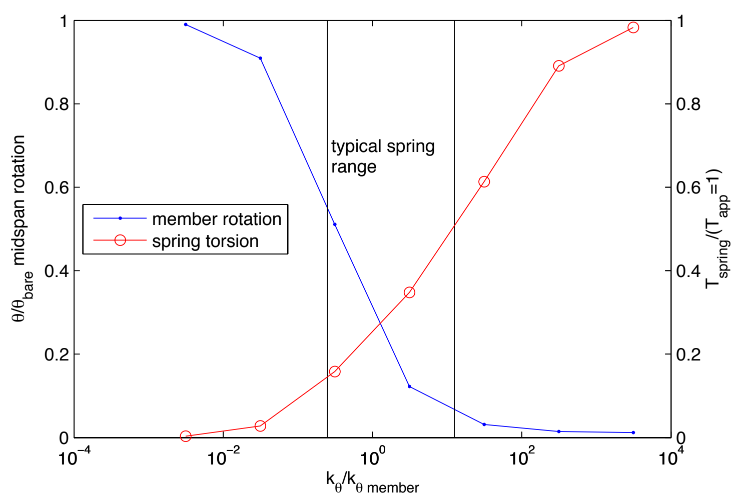

Figure 12 Torsional stiffness analysis depicting member rotation at mid-height and torsion in the mid-height discrete spring as a function of rotational stiffness of the spring normalized by rotational stiffness of the member

It is concluded that a valid alternative to assuming that the fasteners must carry the full torsional demand is to perform a torsional stiffness analysis as conducted here. The impact of this model on the predicted capacities for fastener limit states is investigated in the next section. Additional impacts of such an analysis are a need to examine or limit member rotations, and the reality that direct torsional stresses are introduced into the member.

6.5 – Demands and Fastener Limit States

Stiffness (Figure 6, k_x, k_ϕ) and capacity (Table 5, P_{pt}, P_{br}) are known for the fastener-sheathing systems (i.e., combinations of fasteners and sheathing) tested. For one-sided sheathing, Figure 13a, the only mechanism that can resist torsional demand is the rotational restraint mechanism that includes bearing and pull-through. The torsional moment on face "*i*" (where *i* is either 1 or 2) is

Pull-through related torsional resistance

$$T_{pti}\left(\theta\right) = k_{\phi i}\theta \tag{4a}$$

$$\left(T_{pti}\right)_{\max} = P_{pti}\left(b/2\right) = k_{\phi i}\theta_{pti} \tag{4b}$$

For two-sided sheathing, Figure 13c and Figure 13d, (where "*i*" refers to face 1 and 2), both the pull-through related and bearing related mechanisms may exist, specifically:

Pull-through related torsional resistance

$$T_{pti}\left(\theta\right) = k_{\phi i}\theta \tag{5a}$$

$$\left(T_{pti}\right)_{\max} = P_{pti}\left(b/2\right) = k_{\phi i}\theta_{pti} \tag{5b}$$

Bearing related torsional resistance

$$T_{bri}\left(\theta\right) = k_{xi}\left(d^2/4\right)\theta \tag{5c}$$

$$\left(T_{bri}\right)_{\max} = P_{bri}\left(d/2\right) = k_{xi}\left(d^2/4\right)\theta_{bri} \tag{5d}$$

The total torsional resistance supplied by the fastener-sheathing may either be based on first failure:

Torsional resistance at first failure

$$\theta_f = \min\left(\theta_{pt1}, \theta_{br1}, \theta_{pt2}, \theta_{br2}\right) \tag{6a}$$

$$T_1 = T(\theta_f) = T_{pt1}(\theta_f) + T_{br1}(\theta_f) + T_{pt2}(\theta_f) + T_{br2}(\theta_f) \tag{6b}$$

Or instead may be based on fully ductile failure response in the fastener-sheathing system and thus based on maximum strength

Torsional resistance, fully ductile maximum strength

$$T_2 = \left(T_{pt1}\right)_{\max} + \left(T_{br1}\right)_{\max} + \left(T_{pt2}\right)_{\max} + \left(T_{br2}\right)_{\max} \tag{7}$$

The basic values for face 1 and 2 are provided in Table 6.

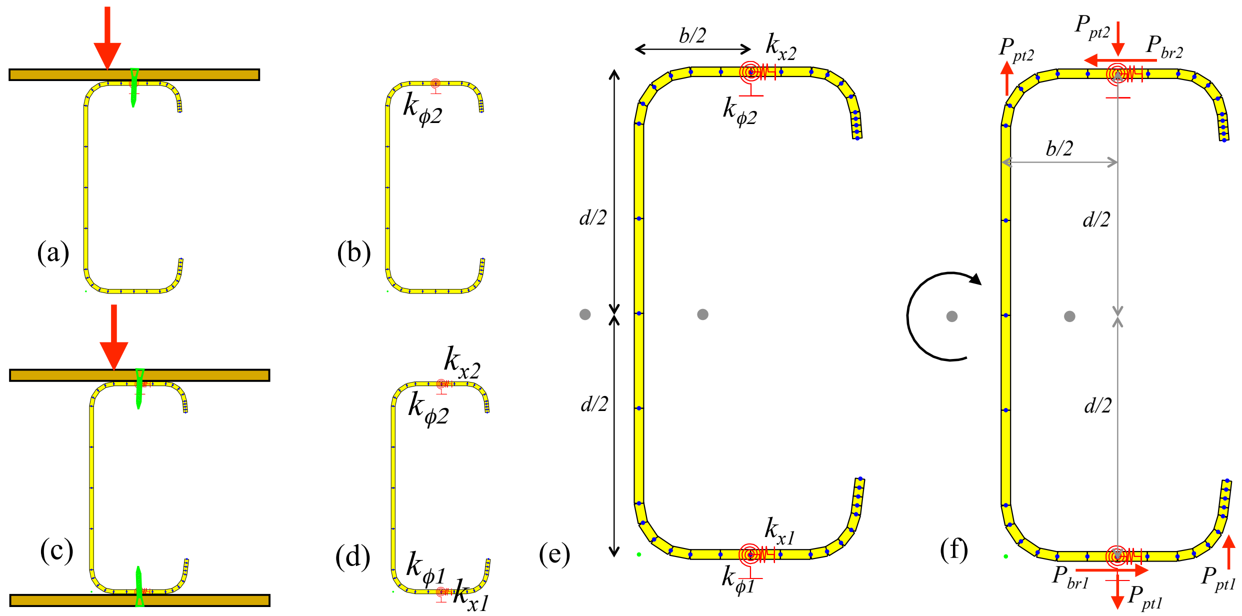

Figure 13 Fastener-sheathing stiffness models for one-sided sheathing (a) one-sided sheathing on loaded face, (b) rotational spring, modeling force couple from bearing into the board and pull-through at fastener, (c) two-sided sheathing, (d) model 1, standard model, including pull-through related (k_ϕ) and bearing resistance (k_x) springs on both faces, (e) model 1, standard model, with springs (f) model 1, standard model with forces (including pull-through (P_{pt}) and bearing (P_{br})

Table 6 Basic strength and stiffness of springs modeling fastener-sheathing system

	face 1: unloaded face/flange in test (flange twists toward board typ.)								face 2: loaded face/flange in test (flange twists away from board typ.)							
sheathing	P_{br1} (lbf)	k_{x1} (kip/in.)	T_{br1} (kip-in.)	q_{br1} (rad)	P_{pt1} (lbf)	k_{f1} (kip-in./rad)	T_{pt1} (kip-in.)	q_{pt1} (rad)	P_{br2} (lbf)	k_{x2} (kip/in.)	T_{br2} (kip-in.)	q_{br2} (rad)	P_{pt2} (lbf)	k_{f2} (kip-in./rad)	T_{pt2} (kip-in.)	q_{pt2} (rad)
BB	-	-	-	-	-	-	-	-	-	-	-	-	-	-	-	-
OB	-	-	-	-	437	0.84	0.35	0.42	-	-	-	-	-	-	-	-
BO	-	-	-	-	-	-	-	-	-	-	-	-	437	0.84	0.35	0.42
GG	86	2.43	0.16	0.02	40	0.85	0.03	0.04	86	2.43	0.16	0.02	40	0.85	0.03	0.04
OG	578	5.52	1.05	0.06	437	0.84	0.35	0.42	86	2.43	0.16	0.02	40	0.85	0.03	0.04
GO	86	2.43	0.16	0.02	40	0.85	0.03	0.04	578	5.52	1.05	0.06	437	0.84	0.35	0.42
OO	578	5.52	1.05	0.06	437	0.84	0.35	0.42	578	5.52	1.05	0.06	437	0.84	0.35	0.42

d = 3.62 in., b = 1.62 in., e = 0.91 in.

For two-sided sheathing three models are considered for the development of the torsional resistance of the fastener-sheathing system: model 1 assumes that both bearing and pull-through related mechanisms are engaged; model 2 assumes that pull-through related mechanisms govern for the unloaded face where the flange twists away from the board and sheathing related mechanics govern for the flange which twists toward the board; model 3 assumes that bearing exists for both flanges, but pull-through only for the loaded flange (face 2) which twists away from the board.

For each model four predicted torsional capacities are investigated, e.g. for model 1:

pred. 1-1 fastener resists full torsional demand, failure at first mechanism, $H_1=T_1/e$
pred. 1-2 fastener resists full torsional demand, max fastener capacities, $H_2=T_2/e$
pred. 1-3 fastener demand from stiffness analysis, failure at first mechanism, $H_3=T_1/T_{spr}/e$
pred. 1-4 fastener demand from stiffness analysis, max fastener capacities, $H_4=T_2/T_{spr}/e$

Table 7 Detailed strength predictions for fastener limit state based failure for three models (see Figure 13)

	model 1:standard model, all springs engaged															
						pred. 1-1		**pred. 1-2**		**analysis (T_{app}=1)**		**pred. 1-3**		**pred. 1-4**		**test**
	k_q	q_f	$T_1=T(q_f)$	$T_2=\mathrm{sum}(T$	$q(T_2)$	$H_1=T_1/e$	q_1	$H_2=T_2/e$	q_2	T_{spr}	q_{mid}	$H_3=T_1/T_{spr}/e$	q_3	$H_4=T_2/T_{spr}/e$	q_4	H^1
sheathing	(kip-in./rad)	(rad)	(kip-in.)	(kip-in.)	(rad)	(kip)	(deg)	(kip)	(deg)	(kip-in.)	(rad)	(kip)	(deg)	(kip)	(deg)	(kip)
BB	-	-	-	-	-	-	-	-	-	-	0.312	**-**	-	-	-	**0.59**
OB	0.84	0.421	0.35	0.35	0.421	0.389	24.14	0.389	24.14	0.14	0.173	**2.711**	24.41	2.711	24.41	**1.120**
BO	0.84	0.421	0.35	0.35	0.421	0.389	24.14	0.389	24.14	0.14	0.173	**2.711**	24.41	2.711	24.41	**1.080**
GG	17.62	0.020	0.34	0.38	0.038	0.379	1.12	0.413	2.18	0.40	0.026	**0.941**	1.30	1.027	1.42	**1.230**
OG	27.73	0.020	0.54	1.59	0.421	0.596	1.12	1.745	24.14	0.45	0.020	**1.320**	1.37	3.865	4.02	**1.380**
GO	27.73	0.020	0.54	1.59	0.421	0.596	1.12	1.745	24.14	0.45	0.020	**1.320**	1.37	3.865	4.02	**1.630**
OO	37.85	0.058	2.19	2.80	0.421	2.406	3.31	3.077	24.14	0.49	0.017	**4.930**	4.26	6.305	5.45	**1.660**

In the corresponding test report to this paper (Peterman and Schafer 2012), model 1 is determined to be most accurate and is the focus of this section. A full analysis of the other models can be found in said rest report. Again, focusing on model 1, consider pred. 1-2 which is the closest to modern strength design assumptions: i.e., torsional resistance is equal to the sum of the mechanisms, and it is assumed that the full torsional demand must be resisted by the fastener. Figure 14a provides the comparison to pred. 1-2, the results indicate that the OB, BO, and GG sheathed conditions should fail around 0.4 kips horizontal force and the OG, GO, and OO should not fail due to fasteners limit states, but rather yielding. The results are not consistent with the test observations and if implemented would lead to excessively conservative capacity predictions based on fastener limit states that do not occur. They do not occur because the stiffness of the fastener-sheathing is not great enough to place all the demand in the fasteners alone.

Model 1, pred. 1-3, would appear to be the most rational choice – the torsional capacity is based on first failure in either pull-through or bearing for either face 1 or face 2 – and the torsional demand is based on a stiffness analysis between the member torsional stiffness and the supplied fastener-sheathing torsional stiffness. Figure 14b provides the results compared with the test data. The one-sided sheathing cases (OB,BO) are not predicted to fail by fastener failure, and indeed they did not, they failed by excessive torsion.

For pred. 1-3 the member with gypsum sheathed on both sides (GG) is predicted to fail at H=0.94 kips – in the tests the member was able to sustain 1.23 kips. Although the prediction is conservative it does correctly capture the fact that at high bending demands fastener limit states not member limit states control for the GG case; further, the prediction (and the use of the torsional stiffness analysis) is a significant improvement of pred. 1-1 or 1-2 which leads to GG capacities near 0.4 kips.

For pred. 1-3 the two-sided sheathing cases with OSB: OG, GO, OO are not predicted to be controlled by fastener limit states; instead member limit states are predicted to control. The accuracy of this is somewhat difficult to judge in the tests, as the members yield in bending the torsional member resistance decreases and eventually fastener limit states are observed. It is postulated the fastener limit states occur after the member limit state, but this is not proven by the available observations.

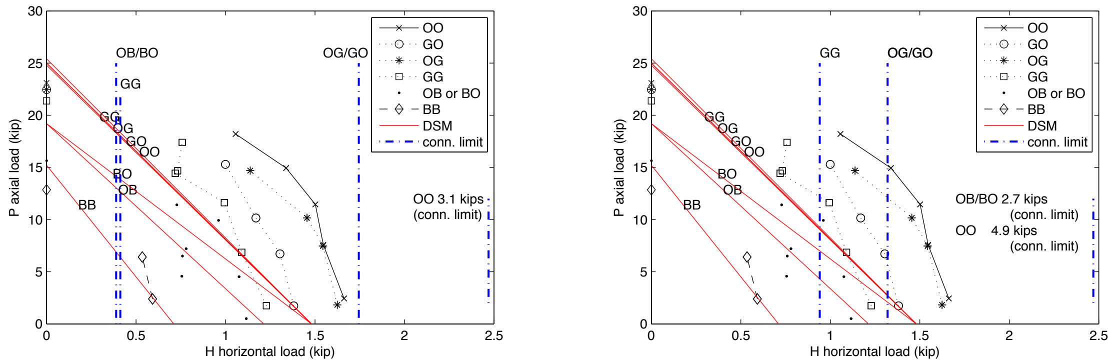

(a) (b)

Figure 14 P vs. H summary plot of Figure 10 augmented with fastener limit states (a) pred. 1-2 fastener limit states based on maximum strength AND all torsion assumed to be carried in the fastener, (b) pred. 1-3 fastener limit state based on first failure (bearing or pull-through) and fastener demands based on torsional stiffness analysis as depicted in the previous section.

7. Conclusions

Testing and analysis is conducted on a 8 ft. high 362S162-68 (50 ksi) stud connected to 362T162-68 (50ksi) track with varying combinations of oriented strand board (O), gypsum board (G) and bare/no sheathing (B) connected to the two flanges and subject to axial load (*P*) and a directly applied horizontal load (*H*) to induce major-axis bending of the stud (and torsion due to the shear center of the stud). The results demonstrate that sheathing has a definitive and positive impact on the stability and strength of the stud. One-sided sheathing cases (OB and BO) significantly increase the strength above no sheathing (BB), but the applied horizontal load induces significant torsion and the stud is essentially limited by serviceability/excessive twist. Two-sided sheathing cases (with one exception) develop their full member capacity and show a clear progression in capacity with two-sided gypsum board (GG) being the weakest, and the strength increasing with the mixed cases from OG to GO up to the two-sided OSB (OO), which is the strongest.

Deformations at the stud-fastener-sheathing locations are a dominant visual portion of the observed response as the sheathing attempts to stabilize the stud against torsion demand (*He*) developed from the horizontal load *H* being applied by direct bearing and thus a distance *e* away from the shear center. In the testing the descending branch of the strength response typically initiates when pull-through of the center fastener through the sheathing is observed; however, comparison against the member strength for all the two-sided sheathing cases (excepting GG) shows that this fastener failure does not precipitate the failure, but rather occurs after the specimen has developed its bending yield capacity (and presumably is weakening, thus increasing demands to the fasteners). In the gypsum sheathed case the pull-through failure occurs before the member reaches full yield. It is further shown herein that none of the fastener-sheathing combinations utilized herein completely restrict torsion in the stud – as a result accurately determining the fastener demands to assess fastener limit states requires a torsional stiffness analysis. Such an analysis is demonstrated herein, and it does properly capture the inadequacy of the gypsum-sheathed case when compared against OSB or mixed OSB-gypsum sheathing.

The analysis provided herein provides a means to perform a detailed assessment of a CFS stud wall under axial load and bending with differing sheathing configurations. One first determines the stiffness and strength of the fastener-sheathing system that will be providing resistance to the stud. This may be done by test (preferably) or using simplified closed-formed solutions (previously developed, but conservative). Second, the member stability in local, distortional, and global buckling must then be assessed. This may be done by computational analysis (preferably) or using closed-form solutions (previously developed, but involved). Third, the member stability analyses is used to assess the member limit states using either effective width or Direct Strength Method approaches, Direct Strength Method is demonstrated herein. Direct torsion was not considered in the member limit state analyses performed herein, but is included in the fastener limit states. Fourth, the fastener-sheathing capacities must be determined for pull-through and bearing limit states. The authors were unable to find generally available methods or industry reported values for these limit states and thus instead relied on our own direct testing (previously conducted). Fifth, to determine the fastener demands one may assume all the torsion must be carried by the fasteners or perform a torsional stiffness analysis to determine the proportion carried by the member vs. that carried by the fastener-sheathing combination (preferred). Finally, the minimum of the member and fastener limit states controls the strength.

Cold-formed steel stud walls braced by sheathing and subjected to axial and bending loads can provide the full member capacity (i.e. the local buckling limited strength) if properly detailed. Additional work is needed to simply the design approach and develop procedures for use in everyday design.

Acknowledgments

This paper was prepared as part of the AISI sponsored project: Sheathing Braced Design of Wall Studs. The project also received supplementary support and funding from the SSMA. Any opinions, findings, and conclusions or recommendations expressed in this publication are those of the author(s) and do not necessarily reflect the views of AISI, nor SSMA.

References

Li, Z., Schafer, B.W. (2010) “Buckling analysis of cold-formed steel members with general boundary conditions using CUFSM: conventional and constrained finite strip methods.” Proceedings of the 20th Int’l. Spec. Conf. on Cold-Formed Steel Structures, St. Louis, MO. November, 2010.

Peterman, K. D., Schafer, B.W. (2012), “Experiments on the Stability of Sheathed Cold-Formed Steel Studs Under Axial Load and Bending: A Test Report.” Available at <http://www.ce.jhu.edu/bschafer/sheathedwalls/index.htm>

Schafer, B. W., Vieira Jr., L. C. M., Sangree, R. H., Guan, Y. (2010) "Rotational Restraint and Distortional Buckling in Cold-Formed Steel Framing Systems." Revista Sul-Americana de Engenharia Estrutural (South American Journal of Structural Engineering), Special issue on cold-formed steel structures, 7 (1) 71-90.

Steel Stud Manufacturers Association (SSMA) (2010) Product Technical Information.

Vieira Jr., L. C. M., Schafer, B.W. “Lateral Stiffness and Strength of Sheathing Braced Cold-Formed Steel Stud Walls.” Elsevier, *Engineering Structures.* (Accepted 2011).

Vieira Jr., L. C. M., Shifferaw, Y., Schafer, B.W. (2011) “Experiments on Sheathed Cold-Formed Steel Studs in Compression.” Elsevier, *Journal of Constructional Steel Research.* 67 (10) 1554-1566 (doi:10.1016/j.jcsr.2011.03.029).

Shifferaw, Y., Vieira Jr., L.C.M., Schafer, B.W. (2010). “Compression testing of cold-formed steel columns with different sheathing configurations.” *Proc. of the Structural Stability Research Council - Annual Stability Conference*, Orlando, FL. 593-612.

Vieira Jr., L.C.M (2011). “Behavior and Design of Sheathed Cold-Formed Steel Stud Walls Under Compression." Doctoral Dissertation submitted to Johns Hopkins University.